Journal of Science and Technology – Engineering and Technology for Sustainable Development
Volume 36, Issue 2, April 2026 , 028–035

Organic Dyes and Perfluorooctanoic Acid Decompositions by Cerium- and Copper-Modified Commercial TiO_2 under Visible Light

Nguyen Quynh Vi, Truong Minh Thu, Do Thi Thanh Thao, Nguyen Ngoc Mai*
Hanoi University of Science and Technology, Ha Noi, Vietnam
**Corresponding author email: mai.nguyenngoc@hust.edu.vn*

Abstract

The study focuses on doping low-cost commercial TiO_2 (P25) to synthesize composite photocatalysts, Cu/TiO_2 and Ce/TiO_2, which decompose organic dyes and perfluorooctanoic acid (PFOA) under mostly visible light of a Xenon lamp. By the basic impregnation method, copper and cerium are successfully doped in P25 with different contents, which is confirmed by some structural analysis, such as X-ray analysis, inductively coupled plasma optical emission spectroscopy, and scanning electron microscopy. The optical band gaps of P25, Cu/P25/1, Cu/P25/5, Ce/P25/1, and Ce/P25/5 are respectively 3.10, 2.96, 2.93, 2.84, and 2.92 eV. Under the Xenon lamp illumination (300-700 nm, 95% visible light), the decomposition ability of Ce/P25/1 with organic dye is the best, 96.7% methylene blue decomposition after 30 minutes, and methyl orange is 90.4% after 50 minutes. The study also looks at how different types of dyes affect the ability of the photocatalysts to break down substances by examining how well the photocatalysts can adsorb the dyes. Moreover, about 22.6% of PFOA is degraded by Ce/P25/1 under the Xenon lamp illumination (300-700 nm, 95% visible light). Therefore, this research compares photocatalytic materials synthesized from cheap commercial sources to decompose pollutants in water, contributing to the development of wastewater treatment technology in Vietnam.

Keywords: Composite photocatalysts, perfluorooctanoic acid, wastewater treatment, titanium dioxide.

1. Introduction

Organic dyes (ODs) and perfluorooctanoic acid (PFOA) are popular contaminants in water, identified by their toxicity and long-term persistence in the environment. Due to the strong carbon-fluorine bonds, PFOA exhibits high stability and resistance to conventional chemical, biological, and thermal degradation processes [1]. Furthermore, it has the potential for bioaccumulation, which can lead to adverse effects on ecosystems and human health. PFOA has been reported to exhibit endocrine toxicity, impair liver function, and increase the risk of cancer when present in the bodies of humans or animals [1]. Similarly, organic dyes from the textile, printing, and dyeing industries pose significant environmental difficulties because of their complex aromatic compounds. ODs not only color the water, but they also limit light penetration, preventing photosynthesis and damaging aquatic life. In addition, ODs are carcinogenic and mutagenic, providing direct dangers to human health through contaminated drinking water and food systems [2]. The remediation of water pollution has become increasingly imperative due to growing civilization and industrialization.

Advanced oxidation processes (AOPs) represent water treatment technologies that produce highly oxidative free radicals, including hydroxyl radicals, for decomposing recalcitrant pollutants [3]. The water treatment method known as photocatalysis emerges as a promising solution because it produces strong hydroxyl and superoxide free radicals when exposed to light [3]. These free radicals can break down sturdy chemical bonds, such as the fluorocarbon chains in PFOA or the double bonds in the dye structures, and transform them into safer products like CO_2, H_2O, or inorganic ions [4]. Photocatalysis has no chemical requirement, only utilizing sunlight or UV light as the energy source, thereby minimizing the generation of harmful byproducts and ensuring sustainability. Moreover, photocatalysts are effective against many toxins and contaminants, with potential for widespread application, especially P25. P25 is a widely used commercial form of TiO_2, notable for its superior characteristics, including a large surface area, an optimal anatase-rutile ratio, and high photocatalytic activity [5]. As a result, P25 plays a crucial role in generating radicals, which can break down the sturdy bonds and decompose the complex structures of FPOA or OD into less toxic products. However, the photocatalytic efficiency of P25 remains limited because it requires high energy to operate under visible light conditions [5]. Additionally, the fast recombination of electron-hole pairs also decreases the generation of strong oxidizing radicals, which limits the treatment efficiency of pollutants. Therefore, in recent years, there have been many studies related to improving P25 photoactivity.

Metal-doped P25 upgrades photocatalytic performance via multiple types of approaches, including

p-ISSN 3093-3242
e-ISSN 3093-3579
https://doi.org/10.51316/jst.189.etsd.2026.36.2.4
Received: Jun 12, 2025; Revised: Aug 26, 2025;
Accepted: Sep 4, 2025; Online: Mar 23, 2026.

bandgap narrowing, greater visible light absorption, and diminished electron-hole pair recombination. Transition metals such as Fe, Cu, and Ag are commonly used to modify TiO_2 on account of their ability to create intermediate electron-trap states, which improve charge separation efficiency [6]. On the other hand, noble metals (Pt, Au, and Pd) are similar to electron capture centers, increasing the material's redox potential [7]. Doping P25 with copper (Cu) and cerium (Ce) has been extensively explored, with several promising results in terms of photocatalytic efficiency. Cu doping of P25 improves visible light absorption by introducing intermediate energy levels within the band gap and inhibiting electron-hole pair recombination. For instance, previous studies have revealed that doping TiO_2 with 1-3 wt.% Cu boosts its photocatalytic capability for organic pollutant degradation [8, 9]. Similarly, cerium (Ce), a rare earth metal that can move between Ce^{3+} and Ce^{4+} oxidation states, supports electron capture efficiency and catalytic efficiency. The previous research showed that Ce doping of 0.5 – 2 wt.% considerably improved the decomposition efficiency of methylene blue (MB) under visible light irradiation [10]. Thus, Cu and Ce are commonly used to modify TiO_2 since they introduce intermediate states in the band gap and have strong electrical conductivity, permitting efficient electron separation and transmission. These processes diminish electron-hole recombination and increase the lifespan of reactive species, thereby increasing P25's photocatalytic performance.

The main objective of the study is to improve the photocatalytic performance of P25 by doping cerium and copper with different ratios. The photoactivity of catalysis is evaluated through PFOA and OD degradation under mostly visible light from a Xenon lamp (300 – 700 nm). By a simple impregnation process, P25/Cu/*x* and P25/Ce/*x* (*x* is the weight percentage of Cu or Ce in the sample) were successfully synthesized. The Cu and Ce percentages were determined by elemental analysis through inductively coupled plasma optical emission spectroscopy (ICP/OES). The successful synthesis was evaluated and confirmed by X-ray structure analyses such as X-ray diffraction (XRD) and X-ray photoelectron spectroscopy (XPS). The catalyst particle powders were also observed by scanning electron microscopy (SEM) with some magnifications. UV-vis diffuse reflectance spectroscopy (UV-DRS) spectra of catalysts are investigated. Then, the samples' optical band gap is determined. Under Xenon lamp illumination (300 – 700 nm), the catalysts in the study can decompose PFOA and different ODs, including MB and methyl orange (MO). UV-Vis spectra and photometric measurements allowed the quantification of ODs over time. Meanwhile, the PFOA concentrations before and after catalytic degradation were determined by high-performance liquid chromatography with mass spectroscopy (HPLC–MS). As a result, this study shows particular properties of the P25-based catalyst, alongside a preliminary evaluation of the photocatalyst's potential for breaking down PFOA and OD in water, providing data for improving P25 studies in the future.

2. Materials and Methods

2.1. Materials

Cerium(III) nitrate hexahydrate ($Ce(NO_3)_3.6H_2O$, powder) and copper(II) nitrate trihydrate ($Cu(NO_3)_2.3H_2O$, powder), Perfluorooctanoic acid ($CF_3(CF_2)_6COOH$, 95%), and ammonium acetate ($CH_3CO_2NH_4$, 99.99%) were purchased from Sigma-Aldrich. Titanium dioxide (P25, white powder, anatase-rutile phase mix) was obtained from Evonik. MB (powder), MO (powder), and methanol (CH_3OH, 99.99 %) were provided by Merck.

2.2. Methods

2.2.1. The methods for P25–based catalysts synthesis

The preparation of cerium- and copper-doped commercial titanium dioxide (P25) via the impregnation method involved five steps, as illustrated in Fig. 1, [11]. Prior to synthesis, P25 was dried at approximately 90 °C for 4 hours. Initially, aqueous solutions of cerium nitrate and copper nitrate were prepared. Subsequently, P25 was added to these solutions at metal-to-P25 weight ratios of 1% and 5%, respectively. The resulting mixtures were stirred at room temperature for 24 hours. The precipitates were then collected and repeatedly washed with distilled water. After drying at 100 °C for 24 hours, the powders were ground and calcined at 500 °C for 4 hours, with a heating rate of 5 °C/min. Cu/P25/1, Cu/P25/5, Ce/P25/1, and Ce/P25/5 catalysts were obtained after the synthesis process, and their properties with applications are discussed in the next sections.

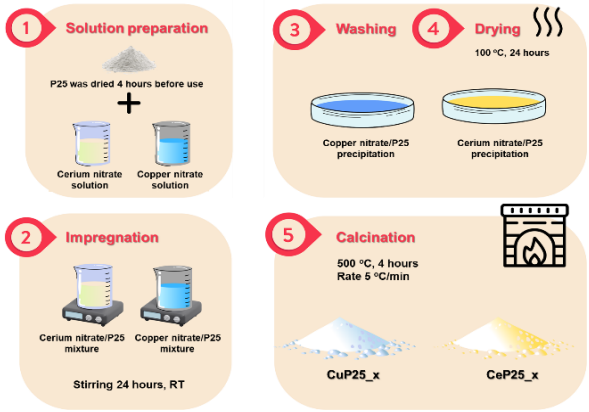

Fig. 1. Schematic overview of photocatalysts preparation by the impregnation method

2.2.2. The methods for catalyst characterization

P25 (reference sample), Cu/P25/1, Cu/P25/5, Ce/P25/1, and Ce/P25/5 are subjected to XRD with the conditions of Cu *kα* radiation (40 kV, 35 mA) on X'Pert Pro (PANalytical) equipment. Cu/P25/1 and Ce/P25/1

are prepared on a stainless-steel holder to analyze XPS by an ESCALAB 220iXL (Thermo Fisher Scientific) with Al $K\alpha$ radiation (E = 1486.6 eV). The measurements are carried out with charge compensation using a flood electron system combining low-energy electrons and Ar^+ ions ($pAr = 1\times10^{-7}$ mbar).

The morphology and energy-dispersive X-ray spectroscopy (EDS) of P25, Cu/P25/1, Cu/P25/5, Ce/P25/1, and Ce/P25/5 are obtained on JEOL JCM-7000 BENCHTOP SEM. The content of Cu, Ce, and Ti in photocatalyst samples was determined by Inductively Coupled Plasma Optical Emission Spectroscopy (ICP/OES) with Varian/Agilent 715-ES.

The UV-Vis spectra of photocatalysts were measured using an Avantes UV-Vis spectrometer. The UV-DRS and the band gap of the samples are determined. This method also showed the concentration of organic dyes (MB and MO) solution before and after photocatalysis.

2.2.3. Investigation of the photocatalytic performance

The decomposition efficiency (*De*) was calculated using the following equation:

$$De\ (\%) = \frac{C_0 - C_t}{C_0}.100 \quad (1)$$

in which, C_0 is the initial concentration of pollutants (OD and PFOA) (ppm), C_t is the concentration of pollutants after t (minutes) of treatment. The pollutant concentration was extrapolated by the standard curve method. For the adsorption and decomposition experiments, the specific conditions were as follows:

Degradation of organic dyes

The photocatalytic performance of samples was studied through the adsorption in the dark and the decomposition under Xenon illumination of MB and MO in water. The UV-Vis analysis was used to determine the residual of MB and MO after treatment by the catalysts.

In the adsorption period, the amount of OD uptake by the catalysts q_t (mg/$g_{catalyst}$) could be calculated according to the following equation:

$$q_t\left(\frac{mg}{g_{catalyst}}\right) = \frac{C_0 - C_t}{m_{catalyst}}.V \quad (2)$$

where V (mL) is the volume of OD's solution, C_0 (ppm) and C_t (ppm) are the initial concentration and the concentration after t (minutes) of OD, $m_{catalysst}$ (g) is the content of samples per test.

In the illumination period by a Xenon lamp (300 – 700 nm), the degradation of OD in an aqueous solution follows a first-order kinetic equation described by the equation:

$$ln\left(\frac{C_0}{C_t}\right) = k_1 t \quad (3)$$

in which C_0 is the initial concentration of OD (ppm), C_t is the concentration of pollutants after the treatment; k_1 is the reaction rate constant (min^{-1}), and t is the time in minutes.

Removal of PFOA

The photocatalytic degradation of PFOA was evaluated using a Xenon lamp (with 5% UV). A 0.2 ppm PFOA solution was prepared using a solution of methanol/ammonium acetate (8/2). 10 ml of PFOA solution of 0.2 ppm at pH about 4 was used to conduct the photoactivity evaluation experiment, which was calculated according to (1), in which, C_0 is the initial concentration of PFOA (ppm), C_t is the final concentration of PFOA after 3 hours of treatment. The PFOA's concentration was determined using HPLC-MS.

3. Results and Discussion

3.1. Characterization of Catalysts

All photocatalyst samples (P25, Cu/P25/1, Cu/P25/5, Ce/P25/1, and Ce/P25/5) were characterized using XRD, as illustrated in Fig. 2. The diffraction peaks of P25 are in good agreement with the anatase and rutile phases of TiO_2. Specifically, the peaks at 25.3°, 37.8°, 48.1°, and 54.0° correspond to the (101), (004), (200), and (105) planes of anatase TiO_2, respectively. These 27.4° and 36.1° peaks also overlap with characteristic planes of rutile TiO_2. The incorporation of copper and cerium did not significantly alter the crystalline structure of P25, indicating that the mixed anatase–rutile phase remained intact, which is beneficial for photocatalytic activity. No distinct diffraction peaks for Cu or Ce were observed in Cu/P25/1 and Ce/P25/1, likely due to their low metal loading. However, at higher metal concentrations (Cu/P25/5 and Ce/P25/5), weak peaks corresponding to copper oxide (35.5°) and cerium oxide (28.6° and 33.2°) were detected, suggesting successful doping at detectable levels, [8, 10].

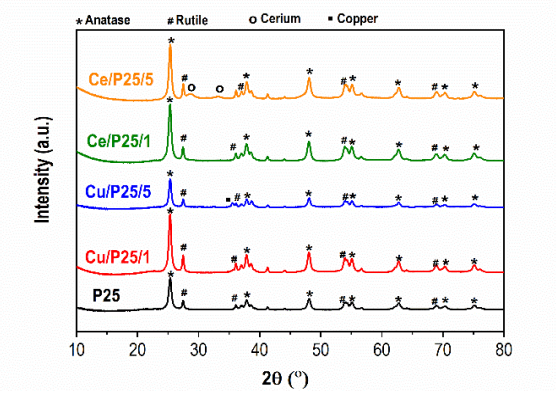

Fig. 2. XRD patterns of P25 and metal-doped P25 with different ratios

While the XRD peak intensity was also partly affected by doping with Ce or Cu. These presences of Ce

and Cu increased the crystallinity of the photocatalyst compared to the original P25, [12]. From XRD data, the catalysts' gain crystallite size is shown in Table 1, which is calculated by the Scherrer equation:

$$CS\ (nm) = \frac{K.\lambda}{\beta.cos\theta} \quad (4)$$

where K is the Scherrer constant (close to 0.9), λ is the X-ray wavelength (nm) of Cu $K\alpha$, β is the full width at the half-maximum intensity of the peak in radians, and θ is the Bragg diffraction angle.

P25's crystallite gain size (*CS*) in this study was 18.4 nm, consistent with the information about Evonik P25. P25 with Cu had a higher *CS* than the original P25; Cu/P25/1 is 20.7 nm and Cu/P25/5 is 20.4 nm. The first explanation might be that the ion Cu^{2+} speeds down the rate of recrystallization, which leads to larger crystals forming when calcined. Furthermore, Cu may be partially contained in oxide form, which might reduce the degree of distortion of the lattice and encourage the growth and enlargement of anatase crystals. In addition, the crystal size decreases as Cu doping increases. This is understood to be too much Cu, generating significant lattice distortion and lattice entanglement, which inhibits crystal formation and produces smaller crystals [12].

The CS of Ce/P25/1 and Ce/P25/5 decreased compared to the original P25 (17.1 and 16.7 nm). This reduction is attributed to the relatively large ionic radius of Ce^{4+}/Ce^{3+}, which induces lattice distortion and disrupts the orderly arrangement of TiO_2 crystals. Moreover, cerium can introduce oxygen vacancies due to its ability to exist in dual valence states (Ce^{4+}/Ce^{3+}), generating defect sites that hinder crystallization and suppress crystal growth [13]. As a consequence, Ce inhibits crystallization through adding internal stress to the TiO_2 lattice, in contrast to Cu, which promotes crystal development.

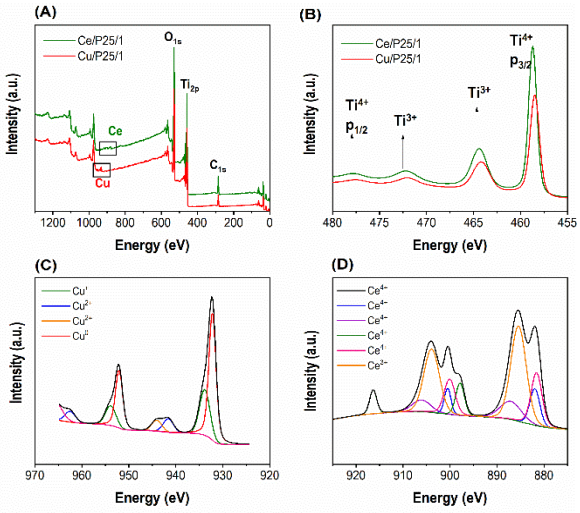

Fig. 3. (A) XPS spectra of metal-doped P25 1% and the high-resolution spectra of (B) Ti2p, (C) Cu, and (D) Ce3d

To further explore the oxidation states of metal elements, Ce and Cu in the doped catalysts, XPS was performed on the P25/Ce/1 and P25/Cu/1 samples, which are presented in Fig. 3. As shown in Fig. 3A, in addition to the fundamental signals such as C1s (298 eV), O1s (533 eV), and Ti2p (458 eV), the signals corresponding to Ce and Cu were also detected, confirming the successful incorporation of the dopants into P25. However, these signals were relatively weak due to the low doping concentration. The high-resolution Ti 2p spectrum (Fig. 3B) shows characteristic peaks of Ti orbitals consistent with Ti^{4+} and Ti^{3+} in TiO_2. Fig. 3C presents the high–resolution XPS spectrum of copper, which reveals Cu^{+} (932 eV) and Cu^{2+} (934–935 eV), [8]. So, the presence of Cu in the Cu^{+} form is expected on the above CS trend reasonably. The oxide form of Cu in the photocatalyst increased the crystallite size. Besides, the high-resolution XPS of cerium is shown in Fig. 3D, which shows Ce^{4+} peaks and Ce^{3+} peaks at 896 and 904 eV, [14].

3.2. Morphology of Catalysts

According to the literature, the crystal form of the Evonik P25 catalyst is similar to that of the anatase phase, [12]. Their morphology may differ from that of normal 100% anatase TiO_2 due to the presence of the rutile phase.

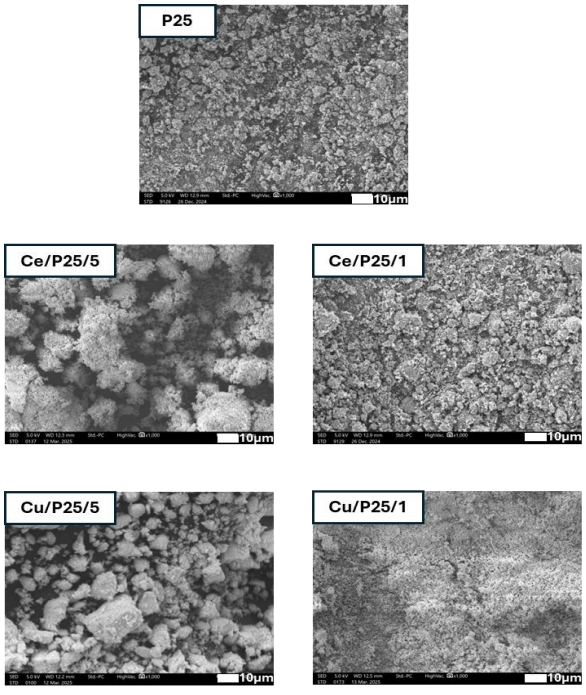

Fig. 4. SEM images of all photocatalysts with magnification x1000

It is evident that while the size of the crystallite clustering region changes dramatically with the addition of metals (Cu and Cu) and P25, the form of the particles does not. Fig. 4 shows that the photocatalyst tends to get larger when metals are added (Table 1). The Cu/P25/1,

Cu/P25/5, Ce/P25/1, and Ce/P25/5 were subjected to elemental analysis by energy dispersive spectroscopy (EDS) and inductively coupled plasma optical emission spectroscopy (ICP/OES) methods, which are shown in Table 1.

Table 1. Summary results of photocatalysts

	P25	Cu/P25/1	Cu/P25/5	Ce/P25/1	Ce/P25/5
Crystallite gain size (nm)	18.4	20.7	20.4	17.1	16.7
E_g (eV)	3.10	2.96	2.93	2.84	2.92
% Metal (ICP/OES)	–	%Cu = 1.8	%Cu = 4.7	%Ce = 0.4	%Ce = 4.4
% Metal (EDS)	–	%Cu = 0.8	%Cu = 4.6	%Ce = 0.9	%Ce = 4.6

3.3. Photoactivity of Catalysts

The UV-DRS spectra of the catalyst samples used in this investigation are presented in Fig. 5. It is apparent that P25 showcases significant UV activity, whereas catalysts added with Cu, Ce at 1% and 5% do not significantly change the catalyst's energy band. However, the photocatalyst's optical band gap has been reduced by the incorporation of Cu and Ce. The optical band gaps of P25, Cu/P25/1, Cu/P25/5, Ce/P25/1, and Ce/P25/5 are respectively 3.10, 2.96, 2.93, 2.84, and 2.92 eV. The Ce^{3+}/Ce^{4+} and Cu^{+}/Cu^{2+} redox couples serve as electron–hole traps, temporarily capturing photogenerated charges and thus slowing down their recombination. For example, Ce^{4+} can capture an electron to form Ce^{3+} ($Ce^{4+} + e^{-} \rightarrow Ce^{3+}$), while Cu^{2+} can be reduced to Cu^{+} ($Cu^{2+} + e^{-} \rightarrow Cu^{+}$); these reduced species are subsequently re-oxidized by oxy (O_2), producing reactive oxygen species (ROS) such as superoxide radical and hydroxyl radical. Overall, this dual role of charge trapping and oxygen activation contributes to narrowing the band gap and enhancing the photocatalytic activity of the doped P25 samples. Since the energy of the orbital 4f of Ce is so near the conduction band, they provide shallow impurity levels in P25 that are readily stimulated by low-energy photons [15]. Consequently, the E_g values drop more precipitously. Moreover, because of the ease of the transition process between Ce^{3+} and Ce^{4+} and the associated charge imbalance, more oxygen defects are formed than in Cu. As a result of these oxygen shortages, the E_g of Ce samples is significantly lower than that of Cu samples.

The adsorption capacity of organic dyes, MB and MO of the photocatalyst samples are shown in Fig. 6. With MB, it can be seen in Fig. 6A that the adsorption capacity of the Ce/P25/1 and Ce/P25/5 samples is much superior, q_t reaching 2.29 and 2.28 mg/$g_{catalyst}$ after 40 minutes of adsorption in the dark. Meanwhile, under the same conditions, P25 has a maximum adsorption capacity of only 0.95 mg/$g_{catalyst}$. An interesting point is that the Cu/P25/1 and Cu/P25/5 samples have much lower q_t values, only 0.40 and 0.89 mg/$g_{catalyst}$.

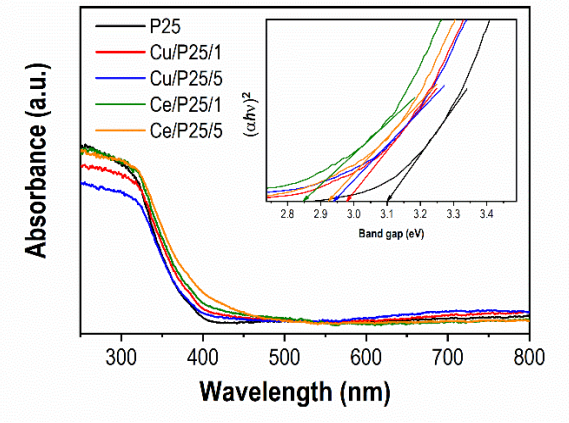

Fig. 5. UV-DRS spectra of photocatalysts; inset: Tauc plots obtained from Tauc's equation to determine the indirect bandgap energies of five samples

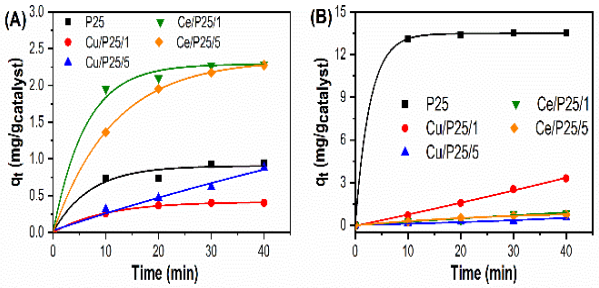

Fig. 6. The adsorption capacity of the five samples with MB (A) and MO (B)

This decrease in adsorption capacity may be due to the fact that Cu has agglomerated quite a lot and causing a reduction in surface area. Ce doping creates more oxygen defects, which act as new active centers, better adsorbing MB. The Ce/P25/1 and Ce/P25/5 samples have smaller crystal sizes and smaller particles, so it can be predicted that the larger surface area results in significantly increased adsorption capacity.

With MO, the maximum adsorption capacity of the photocatalyst samples is shown in Fig. 6B. It is easy to observe that the MO adsorption capacity of P25 (about 13.5 mg/$g_{catalyst}$) is higher than the MB adsorption capacity due to the molecular structure of the MO. MO is negatively charged; it creates an electrostatic repulsion between the catalyst surface and the dye molecules, but MO has a strong interaction with the sulfonate group and the hydroxyl surface of TiO_2 [16]. This leads to a boost in MO adsorption. When doping metal such as Cu and Ce in TiO_2, the photocatalyst surface is coated with metal, leading to a reduction in the interaction of the sulfonate group of MO and the hydroxyl of P25. Without this interaction, there is almost only a weak Van der Waals interaction, which is not strong enough to hold MO on the catalyst surface. Therefore, the q_t value of MO adsorption of Cu/P25/1, Cu/P25/5, Ce/P25/1, and Ce/P25/5 decreased compared

to P25. To improve the adsorption of pollutants in water, the catalyst can be immobilized within a membrane with superior filtration performance. For instance, a regenerated cellulose membrane not only enhances the adsorption capacity of the material but also secures the photocatalytic powder, facilitating its recovery and reuse [17]. Moreover, the transparency of the membrane can be adjusted so as not to compromise the photocatalytic process. Therefore, the photocatalytic material in this study has the potential to be integrated with supporting membranes for water treatment, leading to the development of new materials that are both environmentally friendly and aligned with the circular economy.

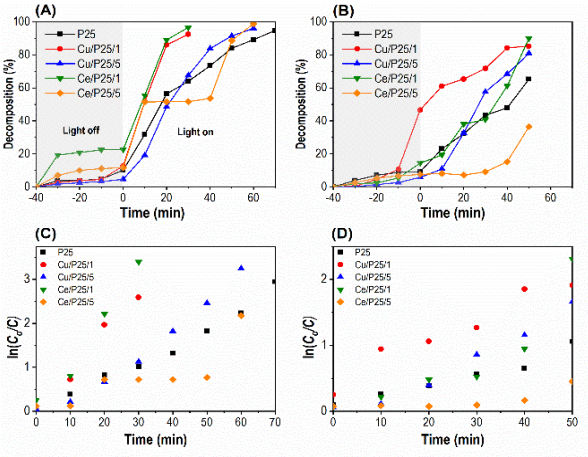

Fig. 7. Degradation efficiency of samples under illumination of a Xenon lamp with MB (A), MO (B), and the relationship curve of $ln(C_0/C)$ and t with MB (C), MO (D)

Fig. 7A shows the decomposition efficiency of MB after 70 minutes of illumination of five photocatalyst samples. P25 is used as a control sample to compare the efficiency of metal doping on TiO_2. P25 almost completely decomposes MB after 70 minutes of illumination with a Xenon lamp. It can be observed in Fig. 7A that 5% metal-doping samples have better performance, for example, Cu/P25/5 can decompose more than 90% of MB after only 60 minutes, while Ce/P25/5 decomposes up to more than 95% of MB at the same time. So, Ce doping has better photocatalytic performance than Cu at the same concentration. It is worth noting that the catalyst samples with a lower metal doping ratio, specifically 1% metal, have better performance. Cu/P25/1 and Ce/P25/1 decomposed 90% and 95% of MB, respectively, after 30 min of illumination under the same conditions. The relationship curve of $\ln(C_0/C)$ and t was shown in Fig. 7C, and the rate constant of the MB decomposition reaction was also determined, as shown in Table 2. The MB decomposition rate of the five samples increased in the order: P25 < Ce/P25/5 < Cu/P25/5 < Cu/P25/1 < Ce/P25/1.

Fig. 7B shows the MO decomposition efficiency of five samples after 50 minutes of illumination. P25 only decomposed about 60% of MO after 50 minutes of illumination with a Xenon lamp. This efficiency is much lower than that of MB (if the same 50 minutes, P25 decomposed more than 80% of MB) because the structure of MO is an anionic dye, unlike MB, which is a cationic dye. On the other hand, as analyzed above, the MO adsorption capacity of catalysts is also very poor, leading to ineffective photocatalysis. It can be observed in Fig. 7B, Ce/P25/5, although doped with the most Ce, is almost ineffective in MO decomposition, and the presence of a lot of Ce here even reduces the MO decomposition efficiency. On the contrary, doping 1% Ce into the Ce/P25/1 sample increases the MO decomposition ability, decomposing about 90 % of MO after 50 minutes of illumination. The same trend also occurred in Cu, 1% Cu doping gave better photocatalytic performance (nearly 90 % MO degradation) than 5% Cu doping (only nearly 80 %). The relationship between $ln(C_0/C)$ and t of MO degradation was shown in Fig. 7D, and the MO degradation reaction rate constant was also determined, as shown in Table 2. The MO degradation rates of the five catalyst samples increased in the order: Ce/P25/5 < P25 < Cu/P25/5 < Ce/P25/1 < Cu/P25/1. A special point to explain here is why 5% Ce doping reduced the photocatalytic performance in MO degradation. According to previous studies, Ce at low concentrations can create defects that are favorable for electron capture and reduce the possibility of electron-hole pair recombination [14]. However, at a 5% doping ratio, clusters of Ce may have formed, creating numerous deep defects that increase the possibility of recombination, thereby reducing the photocatalytic efficiency. In addition, the presence of excessive Ce obscures the photoactive centers, reduces the energy transfer to Ti, and decreases the reaction efficiency.

Table 2. Kinetic parameters for organic dyes' adsorption and degradation

Dyes		Paraments	Units	P25	Cu/P25/1	Cu/P25/5	Ce/P25/1	Ce/P25/5
MB	Adsorption	q_e	$mg.g^{-1}_{catalyst}$	0.966	0.425	0.931	2.321	2.403
		k_{ads}	$g_{catalyst}.mg^{-1}.min^{-1}$	0.453	0.855	0.095	0.405	0.118
	Degradation	k_1	min^{-1}	0.038	0.088	0.048	0.110	0.039
MO	Adsorption	q'_e	$mg.g^{-1}_{catalyst}$	1.357	1.512	1.920	0.778	0.888
		k'_{ads}	$g_{catalyst}.mg^{-1}.min^{-1}$	4.115	0.081	0.233	0.567	0.242
	Degradation	k'_1	min^{-1}	0.019	0.043	0.030	0.033	0.006

Therefore, based on two representative dyes, MB and MO, it can be observed that the 1% doping ratio into P25 exhibited the best performance. This finding is consistent with other scientific reports in the field of dye degradation using photocatalysts [8, 9]. However, it should be emphasized that no single doping concentration can be universally optimal for all pollutants. Each pollutant and each degradation environment may require a different optimal doping level.

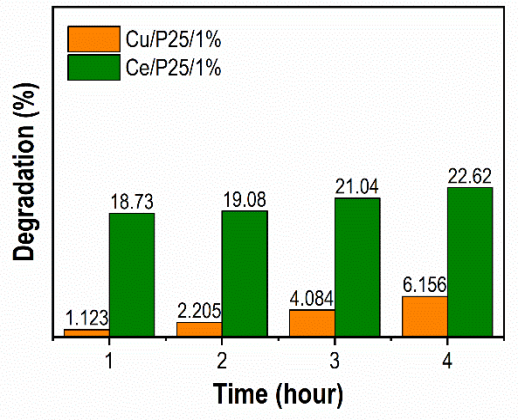

Fig. 8. The PFOA degradation ability of Cu/P25/1 and Ce/P25/1 after illumination for 5 hours

The samples Cu/P25/1 and Ce/P25/1 were selected to test the degradation efficiency of 0.2 ppm PFOA under continuous illumination from a xenon lamp for 5 hours. The results are shown in Fig. 8, with the same illumination time, the efficiency of Ce/P25/1 (22.62%) in decomposing PFOA was superior to Cu/P25/1 (6.156%), but was still low due to the typical limitation of needing more energy to destroy the stable C–F bond. The pKa value of PFOA is 2.8, and the majority of PFOA is in an anionic form in the aqueous solution when pH is larger than 2.8 [1]. From the zeta potential references, the isoelectric point of P25 from Evonik was found to be 6.7. Thus, the catalyst surface will most probably be positively charged when the pH is about 4.5 in this study. Moreover, the Ce/P25/1 surface should be positively charged the favor the adsorption of anionic PFOA ions, which explains the high degradation of PFOA. Recent studies on PFOA degradation using photocatalysis have mostly been published, which have better photocatalytic efficiency when using strong energy light, or adjusting the pH value to increase the decomposition rate of PFOA, for example, a pH of approximately 3, [1]. Therefore, Ce/P25/1 can be integrated with different functionalized materials in water treatment, such as membranes with a cationic surface, to improve the adsorption of PFOA; after that, the pH and light conditions can be fixed to be suitable for increasing the degradation rate.

4. Conclusion

The copper and cerium are successfully doped in commercial TiO_2 at 1% and 5% by the basic impregnation method. Through X-ray analysis, inductively coupled plasma optical emission spectroscopy, and scanning electron microscopy, it can be confirmed that the structure and morphology of commercial TiO_2 rarely changed after doping with metal. In contrast to the structure, the optical band gap of the photocatalyst has a decreasing trend after doping Cu and Ce. As a result, the presence of Cu and Ce changed the adsorption capacity of TiO_2, which can increase the MB adsorption capacity while decreasing the MO adsorption capacity. Doping 1% metal is better than 5%, and doping Ce is better than doping Cu in organic dyes decomposition application, especially Ce/P25/1 can treat 96% MB after 30 minutes and 90% MO after 50 minutes. Ce/P25/1 also had potential in PFOA degradation under visible light, about 22.6 % PFOA can be removed by Ce/P25/1 after 5 hours of treatment.

Acknowledgments

This research was supported by RoHan Project funded by the German Academic Exchange Service (DAAD, No. 57315854), and the Federal Ministry for Economic Cooperation, and Development (BMZ) inside the framework “SDG Bilateral Graduate School Programme”. Quynh Vi Nguyen acknowledges the funding by the Master Scholarship Programme of Vingroup Innovation Foundation (VINIF), code VINIF.2024.ThS.20.

References

[1] J.-M. A. Juve, J. A. D. Reece, M. S. Wong, Z. Wei, and M. Ateia, Photocatalysts for chemical-free PFOA degradation – What we know and where we go from here? Journal of Hazardous Materials, vol. 462, Jan. 2024, Art. no. 132651. https://doi.org/10.1016/j.jhazmat.2023.132651

[2] M. M. Islam, A critical review on textile dye-containing wastewater: Ecotoxicity, health risks, and remediation strategies for environmental safety, Cleaner Chemical Engineering, vol. 11, Mar. 2025, Art. no. 100165. https://doi.org/10.1016/j.clce.2025.100165

[3] P. K. Pandis, C. Kalogiou, E. Kanellou, C. Vaitsis, M. G. Gavvidou, G. Sourkouni, A. A. Zorpas, and C. Argirusis, Key points of advanced oxidation processes (AOPs) for wastewater, organic pollutants and pharmaceutical waste treatment: a mini review, ChemEngineering, vol. 6, iss. 1, Jan. 2022, Art. no. 6010008. https://doi.org/10.3390/chemengineering6010008

[4] P. Kumari and A. Kumar, Advanced oxidation processes for remediation of persistent organic pollutants, Results in Surfaces and Interfaces, vol. 11, Mar. 2023, Art. no. 100122. https://doi.org/10.1016/j.rsurfi.2023.100122

[5] E. Cerrato, E. Gaggero, P. Calza, and M. C. Paganini, The role of Cerium, Europium and Erbium doped TiO2 photocatalysts in water treatment: a mini-review, Chemical Engineering Journal Advances, vol. 10, May 2022, Art. no. 100268. https://doi.org/10.1016/j.ceja.2022.100268

[6] M.-J. Chen, S.-Lien Lo, Y.-C. Lee, and C.-Chieh Huang, Photocatalytic decomposition of perfluorooctanoic acid by transition-metal modified titanium dioxide, Journal of Hazardous Materials, vol. 288, pp. 168–175, May 2015. https://doi.org/10.1016/j.jhazmat.2015.02.004

[7] Y. Chen, Y. Wang, W. Li, Q. Yang, Q. Hou, L. Wei, L. Hiu, F. Huang, and M. Ju, Enhancement of photocatalytic performance with the use of noble-metal-decorated TiO2 nanocrystals as highly active catalysts for aerobic oxidation under visible-light irradiation, Applied Catalysis B: Environmental, vol. 210, pp. 352–367, Aug. 2017. https://doi.org/10.1016/j.apcatb.2017.03.077

[8] B. Hampel, Application of TiO2-Cu composites in photocatalytic degradation of different pollutants and hydrogen production, Catalysts, vol. 10, iss. 1, Jan. 2020, Art. no. 10010085. https://doi.org/10.3390/catal10010085

[9] X.-j. Yang, S. Wang, H. Sun, X. Wang, and J. Lian, Preparation and photocatalytic performance of Cu-doped TiO2 nanoparticles, Transactions of Nonferrous Metals Society of China, vol. 25, iss. 2, pp. 504–509, Feb. 2015. https://doi.org/10.1016/S1003-6326(15)63631-7

[10] C. Alberoni, I. Barroso-Martín, A. I-Molina, E. R.-Castellón, A. Talon, H. Zhao, S. You, A. Vomiero, and E. Moretti, Ceria doping boosts methylene blue photodegradation in titania nanostructures, Materials Chemistry Frontiers, vol. 5, iss. 11, pp. 4138–4152, Mar. 2021. https://doi.org/10.1039/D1QM00068C

[11] K. Zhuang, P. Jin, J. Yao, L. Yu, Z. Sheng, X. Chu, Z. Zhuang, and X. Chen, Different morphologies on Cu–Ce/TiO2 catalysts for the selective catalytic reduction of NOx with NH3 and DRIFTS study on sol–gel nanoparticles, RSC Advances, vol. 13, iss. 37, pp. 25989–26000, Sep. 2023. https://doi.org/10.1039/D3RA03018K

[12] V. Krishnakumar, S. Boobas, J. Yayaprakash, M. Rajabooopathi, B. Han, and M. L-Kultanen, Effect of Cu doping on TiO2 nanoparticles and its photocatalytic activity under visible light, Journal of Materials Science: Materials in Electronics, vol. 27, iss. 7, pp. 7438–7447, Apr. 2016. https://doi.org/10.1007/s10854-016-4720-1

[13] B.-L. Lin, R. Chen, M. -L. Zhu, A. -S. She, W. Chen, B.-T. Niu, Y-Xin. Chen, and X.-M. Lin, Enhanced photoelectrochemical water splitting performance of ce-doped TiO2 nanorod array photoanodes for efficient hydrogen production, Catalysts, vol. 14, iss. 9, Sep. 2024, Art. no. 14090639. https://doi.org/10.3390/catal14090639

[14] E. Bêche, P. Charvin, D. Perarnau, S. Abanades, and G. Flamant, Ce3d XPS investigation of cerium oxides and mixed cerium oxide (CexTiyOz), Surface and Interface Analysis, vol. 40, iss. 3-4, pp. 264–267, Jan. 2008. https://doi.org/10.1002/sia.2686

[15] A. Amritha, M. Sundarajan, R. G. Rejith, and M. A. Mohammed-Aslam, La-Ce doped TiO2 nanocrystals: a review on synthesis, characterization and photocatalytic activity, SN Applied Sciences, vol. 1, iss. 11, Oct. 2019, Art. no. 1441. https://doi.org/10.1007/s42452-019-1455-7

[16] J. Singh and R. K. Soni, Fabrication of hydroxyl group-enriched mixed-phase TiO2 nanoflowers consisting of nanoflakes for efficient photocatalytic activity, Journal of Materials Science: Materials in Electronics, vol. 31, iss. 15, pp. 12546–12560, Jun. 2020. https://doi.org/10.1007/s10854-020-03805-w

[17] V. Q. Nguyen, P. M. Cao, B. C. Nguyen, Thang. M. L., and M. N. Nguyen, Enhancing photocatalytic performance by immobilizing varying TiO2 contents on composite regenerated cellulose membrane: an environmentally reusable membrane, Research on Chemical Intermediates, vol. 51, Aug. 2025. https://doi.org/10.1007/s11164-025-05705-2